# A comprehensive experimental study and numerical modeling of parison formation in extrusion blow molding

Yousefi, Azizeh-Mitra; Collins, Paul; Chang, Stephanie; DiRaddo, Robert W.



**Publisher's version / Version de l'éditeur:**
https://doi.org/10.1002/pen.20662
*Polymer Engineering and Science, 47, 1, pp. 1-13, 2007-01-01*

# A Comprehensive Experimental Study and Numerical Modeling of Parison Formation in Extrusion Blow Molding

**Azizeh-Mitra Yousefi, Paul Collins, Stephanie Chang, Robert W. DiRaddo**
*Industrial Materials Institute, National Research Council of Canada, Boucherville, Quebec, Canada*

**Parison dimensions in extrusion blow molding are affected by two phenomena, swell due to stress relaxation and sag drawdown due to gravity. It is well established that the parison swell and sag are strongly dependent on the die geometry and the operating conditions. The availability of a modeling technique ensures a more accurate prediction of the entire blow molding process, as the proper prediction of the parison formation is the input for the remaining process phases. This study considers both the simulated and the experimental effects of the die geometry, the operating conditions, and the resin properties on the parison dimensions using high density polyethylene. Parison programming with a moving mandrel and the flow rate evolution in intermittent extrusion are also considered. The parison dimensions are measured experimentally by using the pinch-off mold technique on two industrial scale machines. The finite element software BlowParison® developed at IMI is used to predict the parison formation, taking into account the swell, sag, and nonisothermal effects. The comparison between the predicted parison/part dimensions and the corresponding experimental data demonstrates the efficiency of numerical tools in the prediction of the final part thickness and weight distributions. POLYM. ENG. SCI., 47:1–13, 2007. © 2006 Society of Plastics Engineers***

## INTRODUCTION

In the extrusion blow molding process, the first step in the molding cycle is the parison formation. The extruded parison is then inflated to take on the shape of the surrounding mold and finally the part is cooled and ejected. The shape of the parison, especially its diameter and thickness profiles, strongly affects the final part thickness distribution.

*Correspondence to*: A.M. Yousefi; e-mail: azizeh.yousefi@imi.cnrc-nrc.gc.ca
Current address for Paul Collins is Bapco Closures Research Ltd, Millbrook Business Park, Millbrook, Larne, Northern Ireland.
DOI 10.1002/pen.20662
Published online in Wiley InterScience (www.interscience.wiley.com).


Parison swell and sag are factors that significantly influence the parison dimensions. As the polymer melt travels through the die, both shear and elongational stresses are applied to it. Once the melt exits the die in the form of a parison, the stress is relieved. As there are no other forces acting on the parison at this point other than its own weight, parison swell occurs. On the other hand, the gravitational forces acting on the suspended parison cause sag or drawdown. The degree of sag depends on the processing parameters such as melt temperature, suspension time, and total parison length. The combined effect of die swell, parison sag, and die gap programming creates a parison with a nonuniform wall thickness. The degree of swell and sag are controlled by the die design, the extrusion conditions, and the rheological properties of the resin [1].

The most common representation of the parison swell is in terms of the diameter swell ($B_1$) and the thickness swell ($B_2$) defined as

$$B_1 = \frac{D_{\text{parison}}}{D_{\text{die}}} \tag{1}$$

$$B_2 = \frac{h_{\text{parison}}}{h_{\text{die}}} \tag{2}$$

where $D_{\text{parison}}$ and $D_{\text{die}}$ are the parison and die diameters, $h_{\text{parison}}$ is the parison thickness, and $h_{\text{die}}$ is the die gap opening. The final part thickness distribution is directly related to both the diameter and the thickness swell. A section with a larger parison thickness will result in a section with a larger final part thickness, for equivalent blow-up ratios. Also, for equivalent parison thicknesses, a section with a smaller diameter will result in a section with a thinner final part thickness [2]. Therefore, these two parameters can be combined to define the area swell as follows:

$$B_{\text{area}} = B_1 \times B_2. \tag{3}$$

A number of different methods have been employed in the past to measure the parison swell. The earliest studies of parison swell made use of the pinch-off mold originally proposed by Sheptak and Beyer [3]. However, Kalyon

et al. [4] used a photographic technique to show that the pinch-off mold technique may produce unreliable results. DiRaddo and Garcia-Rejon [5] developed a technique for the determination of the parison thickness and diameter profiles in continuous extrusion blow molding by combining the measurements of the parison length evolution with time, the parison diameter profile, the melt flow rate, the axial temperature gradient, and a theoretical description of the effects of swell and sag on the parison. Perhaps the most accurate method to date has been to extrude the parison into an oil bath having the same temperature and density as the melt and to take photographs of the parison at regular intervals [6]. This method enables the determination of swell as a function of time in the absence of sag. However, because of the complexity of this procedure, simpler tests based on the pinch-off mold continue to be used.

The generally accepted understanding is that the parison swell is a viscoelastic phenomenon [7]. The swelling of viscoelastic fluids upon emerging the die can be thought of as a three-step process: a small Newtonian swelling, a sudden elastic recovery, and a further swelling due to stress relaxation [8]. For polymer melts, a main contribution to the extrudate swell comes from the memory effect. This is the elastic response to the elongational stresses prevailing at the entrance of the die. With sufficiently long dies the fluid memory fades almost completely, and an asymptotic swelling ratio is reached [8, 9].

Koopmans [10–12] studied the swelling characteristics of two high density polyethylene (HDPE) resins taken from successive batches of the same commercial grade. He observed that the maximum swell and the time to reach this value are very sensitive to the molecular weight distribution of the resin. He demonstrated the importance of considering the different molecular weight moments to understand the flow behavior of polydisperse polymers. He also reported that small variations in the die or mandrel geometry are usually much more effective in altering the swelling characteristics of an HDPE resin than most of the operating parameters. In light of this, the experimental data collected at a wide range of operating conditions, die geometries, and resin characteristics can also form a basis for finite element simulations, to verify the practical validity of the viscoelastic constitutive equations and the swell prediction models [12].

In general, the maximum extrudate swell is related to the recoverable strain [11]. The Weissenberg number is a quantity that is mostly used to represent the recoverable strain and is defined as follows [2]:

$$\mathrm{WE} = \frac{Q\tau}{A_{\mathrm{die}} h_{\mathrm{die}}} \tag{4}$$

where $Q$ is the volumetric flow rate, $A_{\mathrm{die}}$ is the flow channel area at the die exit, and $\tau$ is the relaxation time represented by the reciprocal of the crossover frequency where the storage modulus ($G'$) and the loss modulus ($G''$) coincide in dynamic shear tests ($G' = G''$) according to the Maxwell viscoelastic model [12].

The goal of this work is to investigate the effects of die design, operating conditions, and resin characteristics on swell and sag. The collected swell data are compared with the numerical prediction of the parison formation using the BlowParison® software developed at IMI. This software has been successfully used in the past to model swell and sag combined with nonisothermal effects for several industrial parts, including fuel tanks [13–15]. The software couples a fluid mechanics approach to represent the die flow, with a solid mechanics approach to represent the parison behavior outside the die. To our knowledge, this approach is the first that is able to yield stable predictions based on the first principles, for high flow rate and small die gap annular systems (high WE numbers).

## THEORETICAL BACKGROUND

Some of the most challenging problems in the numerical simulation of viscoelastic flows are associated with singularities or boundary layers, which occur in the high WE number limit [16]. As a result, the numerical simulation of parison formation in extrusion blow molding remains a challenging task when it comes to high production rates, in particular when high WE numbers are present. The flow of fluids with complex microstructure (e.g. molten polymers) cannot be described by classical Navier–Stokes equations. The stresses in such fluids are determined neither by their current state of deformation nor by their current state of motion; instead, the stresses depend on the whole history of the deformation. Many models exist that are based either on molecular considerations or on modifications of established theories such as linear or nonlinear viscoelasticity [17].

Graham and McLeish [18] investigated the exponential shear flows of polymer melts. In their study, a comparison between the predictions of the "pom-pom" molecular model of McLeish and Larson [19] in exponential shear and experimental data was presented. Accurate quantitative predictions were reported using the multimode approach and the possibility of using exponential shear to obtain the multimode nonlinear spectrum of a melt was explored. In an extensive review, Crochet and Walters [20] presented the numerical simulation of the flow of highly elastic liquids in complex geometries. The need for suitable constitutive models and stable iterative numerical schemes were emphasized, particularly at high WE numbers. Yurun and Crochet [21] developed a high-order elastic–viscous split stress/streamline-upwind Petrov-Galerkin finite element method for simulation of steady viscoelastic flows. The method was applied to the flow of a Maxwell fluid around a sphere. Brasseur et al. [22] solved the time-dependent compressible Newtonian extrudate-swell problem with slip at the wall, in an attempt to simulate the stick-slip extrusion instability. Finite elements were used for the

 DOI 10.1002/pen

space discretization and a standard fully implicit scheme for the time discretization. It was reported that when the volumetric flow rate at the inlet was in the unstable regime and compressibility was taken into account, self-sustained periodic oscillations of the pressure drop and of the mass flow rate at the exit was observed and the extrudate surface became wavy.

Two different approaches exist to calculate the flow stresses for viscoelastic fluids. In the first approach, the flow kinematics is derived using a generalized Newtonian model. The flow kinematics is then used as an input for the viscoelastic equation to calculate flow stresses [23]. In the second approach, namely the direct approach, the viscoelastic behavior of the material is taken into account from the beginning to calculate the flow kinematics [24]. Baaijens [24] compared these methods and concluded that there was a good agreement between the two, while the former was more cost effective. The first approach is adopted in this work to predict the stress experienced by the polymer melt upon the flow in extrusion dies. While the flow kinematics in the die is predicted based on the Hele–Shaw model, assuming Carreau model type behavior for the melt [25], the particle tracking as well as the deformation prediction is preformed using K-BKZ viscoelastic model [26, 27].

### *Flow in the Die*

For a Newtonian fluid, the viscosity is constant. For a fluid obeying the Carreau model used in this work, the viscosity takes the following form [25]:

$$\eta = \eta_0 A_t [1 + (\lambda A_t \dot{\gamma})^2]^{(n-1)/2}. \quad (5)$$

In this equation, $\eta$ is the viscosity of the polymer melt at the processing temperature, $\eta_0$ is the zero-shear Newtonian viscosity at a reference temperature, $A_t$ is the temperature shift factor according to the WLF temperature shift function [28], $\dot{\gamma}$ is the shear rate, $n$ is the power-law index for the shear-thinning zone, and $\lambda$ is a characteristic time representing the transition between the Newtonian and shear-thinning zones. The Newton–Raphson iterative scheme was used to solve the set of equations for the flow kinematics using the Carreau model [29].

### *Parison Formation After Emerging the Die*

The flow kinematics from the flow in the die was used to calculate the flow stresses based on the K-BKZ model. The K-BKZ model is an integral type viscoelastic model that allows the integration of the deformation history in the die based on the particle tracking technique. The overall stress components evaluated for each element were considered as the initial stress being removed at the moment the element emerges from the die. Therefore, the stress relaxation of the semi-solid extrudate was predicted based on the solid-mechanics principles. The K-BKZ model relates the stress to the strain history as follows [26, 27]:

$$\sigma(t) = -q\delta + \frac{1}{1-\theta}\int_{-\infty}^{t} \sum_k [m_k(t-\tau)h_k(\tau,t)] \times \{c^{-1}(\tau,t) + \theta c(\tau,t)\}\, d\tau \quad (6)$$

where $q$ is the hydrostatic pressure, $\delta$ is the identity tensor, $t$ is the time, $\tau$ is the relaxation time, $m$ is the memory function given by the Maxwell relaxation spectrum, $c$ is the Cauchy deformation tensor, $c^{-1}$ is the Finger deformation tensor, $h$ is the damping function based on the Cauchy strain invariants, and $\theta$ is a parameter that refers to the second normal stress difference in the deformation (biaxial effect). The Papanastasiou damping function was used to represent the strain dependency under nonlinear viscoelastic deformation [30, 31]:

$$h_k(t,\tau) = \frac{\alpha}{\alpha - 3 + \beta_k I_1(t,\tau) + \{1-\beta_k\} I_2(t,\tau)} \quad (7)$$

in this equation, $\alpha$ and $\beta$ are the damping coefficients, and $I_1$ and $I_2$ are the invariants of the Finger tensor. The thermal dependence of the K-BKZ model was accounted for with the WLF temperature shift function.

### *Effect of Elongational Forces*

The hybrid fluid mechanics–solid mechanics approach presented in this work is based on the membrane elements for both the flow in the die and parison formation phase, which disregards the three-dimensional nature of the shear flow in the die. Moreover, the presented numerical formulation does not account for the elongational forces developed at the entrance to the die and in the die land area. To compensate for the negative impact of these hypotheses, the hybrid approach is coupled with a mathematical swell model. This model makes use of dimensionless quantities (Weissenberg number and die *L/D* aspect ratio) to compensate for the elongational forces ignored by the hybrid approach.

The swell model identifies a parison recoil factor for each parison programming point, and is developed based on a wide range of experimental trials conducted using different die geometries and operating conditions. Therefore, the overall parison swell predicted for each element at each time-step is a combination of the numerically-predicted swell and the model-based recoil factor (RF), defined as follows:

$$\mathrm{RF} = C_\mathrm{R} \exp\left[S_\mathrm{F} - (S_\mathrm{F} + a_1)\left(\frac{\mathrm{WE_u} - \mathrm{WE}}{\mathrm{WE_u}}\right)^{a_2 D_\mathrm{die}/L_\mathrm{die}}\right]. \quad (8)$$

In this equation, $a_1$ and $a_2$ are constants, $C_\mathrm{R}$ is a die-dependent parameter, $S_\mathrm{F}$ is a resin-dependent swell factor, and $\mathrm{WE_u}$ is a resin-dependent ultimate WE number. The parameter $C_\mathrm{R}$ in *Eq. 8* is a dimensionless parameter that represents the die land contraction ratio and takes the fol-

lowing form:

$$C_R = a_3 + a_4 \left( \frac{\phi_m - \phi_b}{45} \right) \quad (9)$$

where $\phi_m$ and $\phi_b$ are the mandrel and bushing angles, respectively, and $a_3$ and $a_4$ are constants.

In *Eq. 8*, the resin-dependent parameters are estimated by inverse modeling through a comparison between the experimentally-observed parison dimensions and the numerical predictions. It is worth mentioning that based on multitude of experimental observations, these parameters can be linearly related to the ultimate relaxation time of the resin, which is approximated as follows [32]:

$$\tau_u = \eta_0 \frac{\sum_k G_i \tau_i^2}{\left( \sum_k G_i \tau_i \right)^2} \quad (10)$$

where $G_i$ and $\tau_i$ are the relaxation moduli and the relaxation times, respectively, given by the Maxwell relaxation spectrum. A comparison between the predicted parison dimensions (length and thickness) and corresponding experimental values in the following sections demonstrates the efficiency of the developed hybrid approach in predicting the overall parison swell. Further information about the hybrid approach can be found elsewhere [33, 34].

## EXPERIMENTAL

Three commercial HDPE blow molding resins denoted A, B, and C were employed in this study. Table 1 gives the zero-shear Newtonian viscosity ($\eta_0$), the Maxwell relaxation time ($\tau$), and the ultimate relaxation time ($\tau_u$) for these resins (*Eq. 10*). The full relaxation spectrum for these resins can be found elsewhere [34]. The experiments were conducted on two industrial scale intermittent machines featuring different production rates, and consequently different WE numbers.

### *Medium-Shear Intermittent Machine*

An intermittent extrusion machine from PLACO was used in this study. The preliminary tests conducted to determine the flow rate revealed that there was a time delay of 15–20 s, depending on the accumulator ejection speed, before a steady flow rate was achieved. Since the parison swell is flow rate dependent, a series of experiments were initially conducted to obtain the flow rate evolution for each speed. To this end, parisons were extruded for incremental times up to the total extrusion time. The flow rate evolution profile was determined by dividing the parison weights by their respective extrusion times. Each experiment was repeated three times to check for the consistency, and average results were used for this study. Figure 1 shows some of these results as a function of the accumulator ejection speed. Subsequently, the effect of the following parameters on parison swell was examined on this machine. The material type, as well as the operating conditions used for these experiments, is listed in Table 2. The indicated flow rate values are the average flow rates unless specified otherwise.

TABLE 1. Zero-shear Newtonian viscosity ($\eta_0$), Maxwell relaxation time ($\tau$), and ultimate relaxation time ($\tau_u$) at 210°C for the HDPE resins.

| Resin | $\eta_0$ ($10^5$ Pa s) | $\tau$ (s) | $\tau_u$ (s) |
|---|---|---|---|
| A | 0.9 | 0.6 | 37 |
| B | 3.1 | 0.8 | 42 |
| C | 3.3 | 4.2 | 42 |

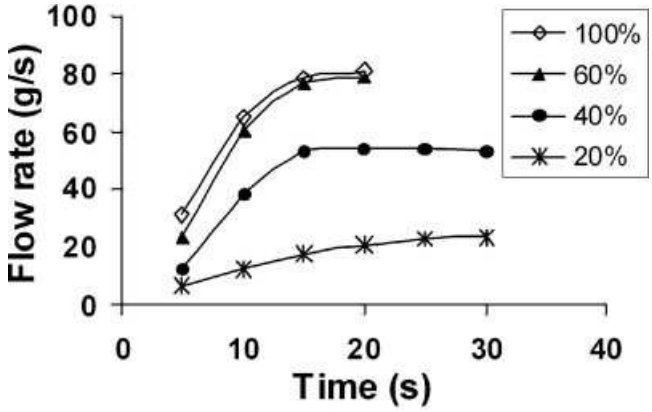


FIG. 1. Flow rate evolution for different accumulator ejection speeds. The speeds are presented as a percentage of maximum ejection speed.

**Die Geometry.** Annular dies with different geometries were used in this study. In all cases, the mandrels used were diverging. Table 3 gives the geometrical information of the dies (I–VI). A die gap opening of 2 mm was used for all these die geometries.

**Die Gap Opening.** Die gap openings of 4 and 6 mm were also set on the dies in Table 3. The mandrel movement required to achieve the desired die gap was calculated based on the mandrel angle. Once the mandrel movement was completed, the horizontal die gap was also physically measured.

**Flow Rate.** To investigate the effect of flow rate on parison dimensions, the experiments were conducted at different machine-set flow rates (32 and 64 g/s). To provide a steady flow rate prior to the pinch-off mold closing, the parison was allowed to extrude for 20 s and was then manually cut off with a pair of scissors. The parison produced after this period was used for the measurements.

**Material Type.** The experiments were conducted using all three of the resins at the steady flow rate of 10 g/s. The extrusion time was varied in order to achieve the target parison length of 250 mm for all of the resins.


DOI 10.1002/pen

TABLE 2. Operating conditions used for the tests.

| Test | Resin | Die[a] | $T_{melt}$ (°C) | Flow rate (g/s) | Die gap (mm) | Extrusion time (s) | WE No. | Parison length (mm) | |
|---|---|---|---|---|---|---|---|---|---|
| | | | | | | | | Exp. | Sim. |
| a | A | I,II,III,IV,V,VI | 210 | 70 ± 5[b] | 2 | 3.8–5.7 | 80–184 | 550 | 575 (IV) |
| b | A | I,II,III,IV,V,VI | 210 | 70 ± 5[b] | 4, 6 | — | 9–37 | 550 | 541, 578 (IV) |
| c | A | III | 210 | 32, 64[c] | 1 | 5.0, 2.7 | 217, 434 | 250 | — |
| d | A, B, C | III | 210 | 10[c] | 1 | 13.4–16.9 | 68–354 | 250 | — |
| e | A, C | III | 210 | 10[c] | 1–2 | 12.5, 13.7 | 5–68 | 250 | 284 (A) |
| f | A | VII | 210 | 67[b] | 0.6, 1.5 | 2.0, 3.5 | 126, 672 | 250 | 242–266 |
| g | A | VII | 210 | 67[b] | 0.6, 1.5 | 3.5, 5.7 | 126, 672 | 500 | — |
| h | A | VII | 200 | 75[b] | 0.8 | 2.5 | 450 | 400 | 424 |

(a–e) medium-shear machine, (f–h) high-shear machine. The experimental and predicted parison lengths are compared for the selected cases.
[a] See Table (3).
[b] Average flow rate during extrusion.
[c] Steady flow rate.

**Parison Programming.** The technique used in industry to control the thickness of the part wall is known as parison programming or die gap programming. The effect of changing the die gap from 1 to 2 mm on the parison thickness profile was investigated using resin A and C at the steady flow rate of 10 g/s. The numerical predictions were compared with the experimental data obtained for resin A.

*High-Shear Intermittent Machine*

The experiments on the high shear intermittent machine were conducted at Petromont Inc. using the die VII in Table 3. The preliminary tests indicated that a steady flow rate was achieved within the first second of the extrusion. Therefore, the flow rate was assumed to be constant during the parison formation. The effect of the following parameters on parison swell was examined. Table 2 lists the operating condition for this series of experiments.

**WE Number.** To investigate the influence of high WE numbers on the parison dimensions, two different die gaps were used at the same flow rate of 67 g/s, targeting the parison length of 250 mm. WE numbers of 126 and 673 were examined.

**Parison Length.** The extrusion time was varied in order to achieve a longer parison for both WE numbers in the previous experiments. A parison length of 500 mm was targeted. These experiments permitted the investigation of the effect of parison length, and as a consequence, the extra parison sag on the final parison dimensions.

**Part Thickness and Weight Profile.** In this series of experiments, the extruded parison was molded into a bottle and the part was subsequently cooled and dissected into thin sections. The thickness and weight profiles of these sections were measured and compared with the corresponding values predicted by IMI's software.

*Parison Dimension Measurements*

The pinch-off mold technique was used to measure the parison dimensions and the weight profile at the end of extrusion for all of the experiments. When the desired length of parison was extruded, the mold closed and formed a series of cushions along the length of the parison. The pinched-off parison was allowed to cool for 48 h before the measurements were taken. The parison was then cut up into their individual cushions and each cushion was weighed and their width and length were recorded. The diameter and thickness swell for each cushion were determined in the following manner:

$$D_{\text{parison}} = \frac{2L}{\pi} f \tag{11}$$

$$h_{\text{parison}} = \frac{w}{2Lh\rho_s} f \tag{12}$$

where

$$f = \left(\frac{\rho_s}{\rho_m}\right)^{1/3} \tag{13}$$

is a function that accounts for the shrinkage, $\rho_s$ and $\rho_m$ are the solid and melt densities, respectively, $L$ is the cushion width, $h$ is the cushion height, and $w$ is the cushion weight. In this study, the overall parison swell is represented either in terms of the diameter and the thickness swell or in terms of the area swell, calculated using *Eq. 3*. Figure 2a shows the quantities used to define the swell parameters. Figure 2b shows an extruded parison after pinch-off.

## NUMERICAL SIMULATIONS

IMI's BlowParison software was used to predict the parison formation, taking into account the swell and sag, as well as nonisothermal effects. In the simulations, a 3-node membrane element was used to create the finite element mesh of the parison (30,000–100,000 elements depending

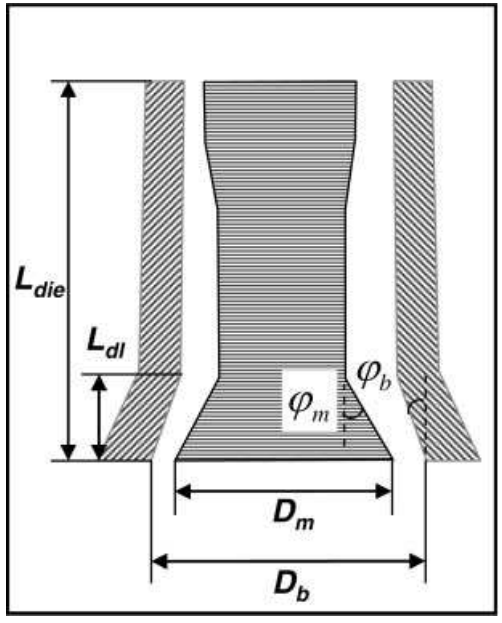


TABLE 3. Die geometries examined in this work.

| Die | Bushing diameter, $D_b$ (mm) | Mandrel diameter, $D_m$ (mm) | Die length, $L_{die}$ (mm) | Die-land length, $L_{dl}$ (mm) | Bushing angle, $\varphi_b$ (degrees) | Mandrel angle, $\varphi_m$ (degrees) |
|---|---|---|---|---|---|---|
| (I) | 25.0 | 23.0 | 41.0 | 6.0 | 0.0 | 45.0 |
| (II) | 36.0 | 35.0 | 88.0 | 6.0 | 45.0 | 45.0 |
| (III) | 40.0 | 38.0 | 41.0 | 6.0 | 0.0 | 45.0 |
| (IV) | 40.0 | 38.0 | 88.0 | 6.0 | 0.0 | 45.0 |
| (V) | 70.0 | 68.0 | 41.0 | 6.0 | 0.0 | 45.0 |
| (VI) | 70.0 | 69.0 | 100.0 | 25.0 | 20.0 | 30.0 |
| (VII) | 80.1 | 79.3 | 130.0 | 46.0 | 20.0 | 24.0 |

DOI 10.1002/pen

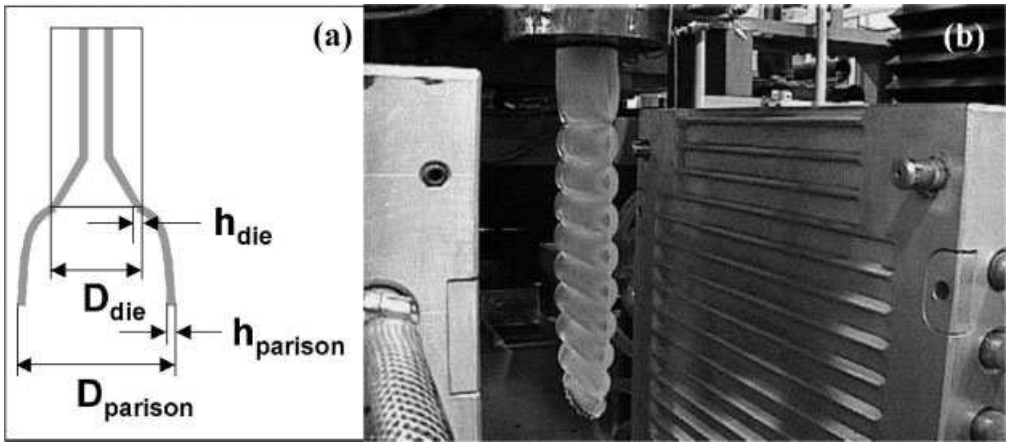


FIG. 2. (a) Quantities used to define the diameter and the thickness swell and (b) extruded parison after pinch-off.

on the parison length). To account for the variable flow rate in intermittent extrusion, the experimental flow rate evolution profiles were used as input data to the software. The parison programming with a moving mandrel was also considered in simulations so as to verify the capability of IMI's software to predict the parison formation for complex parts. In the comparison between the experimental swell data and the numerical predictions, the emphasis was placed either on the area swell or on the weight profile of the pinched-off parison/dissected part. The prediction of the part blowing and clamping for a selected case study was performed using IMI's BlowSim® software [35].

## RESULTS AND DISCUSSION

In this section, the swell profiles along the parison length are calculated using *Eqs. 1–3* and *11–13* and are analyzed so as to relate the observed swell profiles to the relevant geometrical parameters and operating conditions. The experimental parison dimensions and the weight profiles are compared to the numerical predictions for some selected case studies. To make it easier for the reader to compare the swell profiles for the different scenarios presented in this paper, the symbols associated to the data series are displayed at the corner of each Figure in descending order of swell.

### *Medium-Shear Intermittent Machine*

**Die Geometry.** The diameter, thickness, and area swell profiles along the parison length for the dies I to VI are given in Figs. 3a–3c, respectively. As expected from *Eq. 1*, the diameter swell increases as the die diameter decreases with the exception of the die II, which has the same bushing and mandrel angle of 45°. Therefore, the lower diameter swell for this die is attributed to the stronger hoop stresses that tend to reduce the parison diameter after emerging from the die, due to the viscoelastic memory effects [2]. It should be mentioned that the upstream die geometry could also have a pronounced effect on the diameter swell, mainly because the resin tends to regain the upstream diameter at the die exit. A quick look at the images of the dies in Table 3 indicates a much greater changes in the die diameter for the dies I and III (upstream vs. die exit). In light of this, the resulting hoop stresses could be responsible for the increased diameter swell in case of dies I and III (I > III > V). For the dies featuring the same bushing diameters (die III *vs.* IV or die V *vs.* VI), the shorter the die length, the more pronounced the diameter swell. The dependence of the swelling ratio on the die length can be explained by comparing the travel time in the die with the resin relaxation time. For short dies, the travel time is shorter than the resin average memory so that

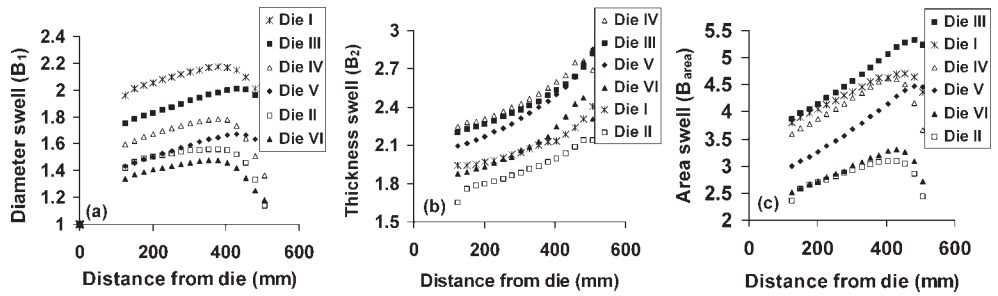


FIG. 3. Effect of die geometry on (a) diameter swell, (b) thickness swell, and (c) area swell for the dies I–VI in the Table 3 (die gap = 2 mm).

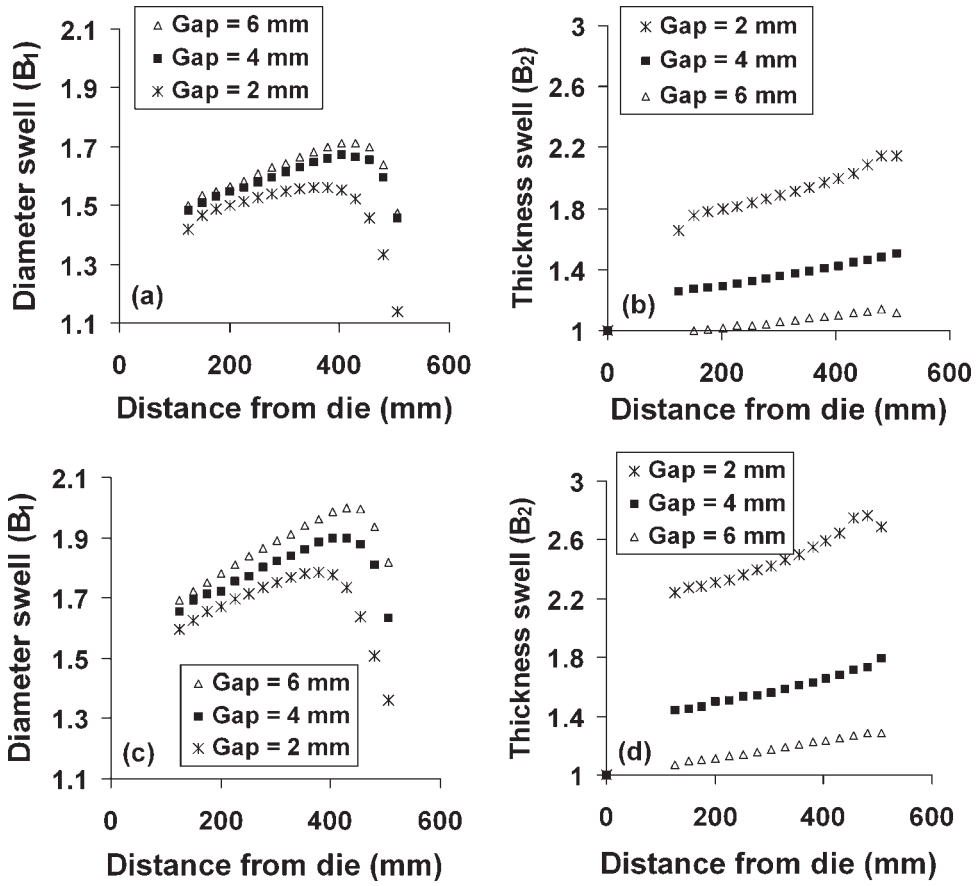


FIG. 4. Effect of die gap opening on (a and c) diameter swell, and (b and d) thickness swell. The die II is used for (a) and (b), and die IV is used for (c) and (d).

an increased swelling is observed as the resin tends to recover the shape it had before entering the die. With sufficiently long dies the resin memory fades almost completely, and an asymptotic swelling ratio could be reached [8].

The thickness swell has a more complex dependence on the die geometry. Although decreasing the bushing angle to zero leads to a higher thickness swell for the dies III, IV, and V (mainly attributed to a more pronounced elongational forces developed at the die land area), the thickness swell shows a much lower value for the die I regardless of the bushing angle. This could be related in part to the upstream die geometry that creates a much higher gap between the bushing and the mandrel compared to the other dies. As a result, lower shear stresses in this area lead to a lower thickness swell. Once again, the die II shows the least swell profile due to the absence of the elongational forces in the die land area, where the bushing and the mandrel are parallel (no contraction). Looking at the global trend of the swell profiles in Fig. 3b, the die length does not seem to affect the thickness swell.

Finally, the overall swell profiles presented in Fig. 3c indicate that the elongational forces, which are directly related to the difference between the mandrel and the bushing angle (contraction), as well as the hoop stresses created in the die land area, have the most significant effect on the overall swell profile. Therefore, a higher extrusion time is

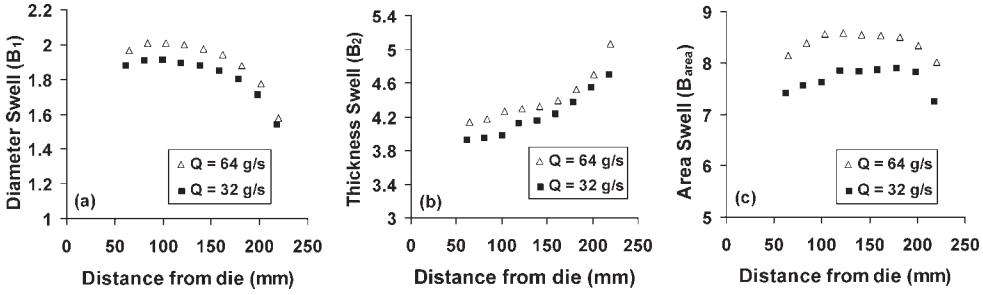


FIG. 5. Effect of flow rate on (a) diameter swell, (b) thickness swell, and (c) area swell using the die III (die gap = 1 mm).

 DOI 10.1002/pen

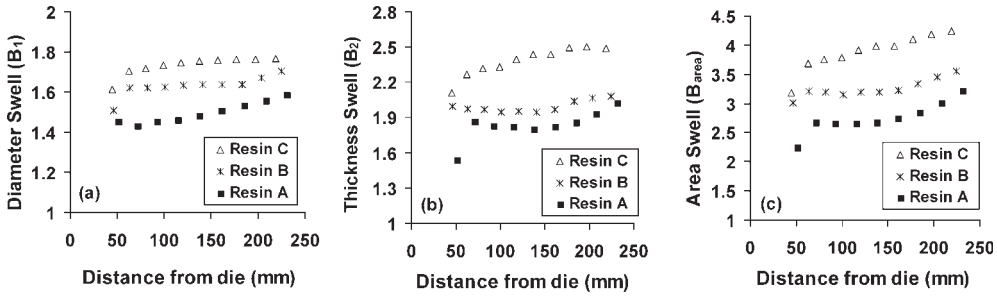


FIG. 6. Effect of material type on (a) diameter swell, (b) thickness swell, and (c) area swell using the die III (die gap = 1 mm).

required using the die III (5.7 s) when compared to the die II (3.8 s) to get the same target parison length of 550 mm.

**Die Gap Opening.** These series of experiments demonstrated that the dies III and IV were the most sensitive to the changes in the die gap opening in terms of the resulting parison swell while the die II was found to be the least sensitive. This can be attributed to the effect of the geometrical parameters discussed in the previous section (see Die Geometry). For the die II, Figs. 4a and 4b show the effect of increasing the die gap opening on the diameter and on the thickness swell, respectively. The corresponding results for the die IV are presented in Figs. 4c and 4d. It can be seen that increasing the die gap reduces the thickness swell in all the cases. This can be explained by the fact that the shear rate in the die, and consequently the recoverable strain, is higher for the smaller die gap.

The results in Fig. 4 also indicate an increase in both the diameter and thickness swell as the distance from die increases, with the exception of the lower-most section of the parison. As the polymer flows further away from the die, its weight imposes less of a constraint, allowing a quasi-free expansion. These results also reinforce the observation made by Graessley et al. [36] that swell occurs in two stages, a very rapid initial swell followed by a slower secondary swell. The lower-most section of the parison shows a less pronounced thickness swell mainly because of the lower flow rates associated to this section in an intermittent extrusion. The resin left in the accumulator from the previous extrusion cycle could also lose its memory to some extent and lead to a lower swell at the bottom of the parison in the following cycle.

**Flow rate.** The effect of flow rate on the diameter, the thickness, and the area swell is shown in Figs. 5a–5c. It can be seen that an increase in flow rate causes an increase in both the diameter and the thickness swell. These observations confirm the results obtained in the die gap opening studies and demonstrate that the parison swell increases as the shear rate increases inside the die.

**Material Type.** The effect of material type on the diameter, the thickness, and the area swell is shown in Figs. 6a–6c. It can be seen that the three resins exhibit three different patterns for both the diameter and the thickness swell. Although the shear rates are similar, there is a large difference in the WE number for each of the resins, ranging from 68 to 354 (see Table 2). As a result, when comparing different resins, the WE number gives a better indication of swell than the shear rate. This way, the swelling behavior of the resin can be directly related to its relaxation time and as a consequence to its level of elasticity. The higher the relaxation time is, the more pronounced the diameter and the thickness swell is because of the increased elastic behavior. The knowledge of the different molecular weight moments of the resin provides insight to its molecular weight distribution and to the amount of large molecules for each resin causing the difference in their swelling characteristics [10]. Once again, the overall swell profiles presented in Fig. 6c indicate that in order to get the same target parison length of 250 mm, a higher extrusion time is required for the resin C (16.9 s) compared to the Resin A (13.4 s).

**Parison Programming.** Figures 7a–7c show the effect of opening the die gap from 1 to 2 mm on the swell pro-

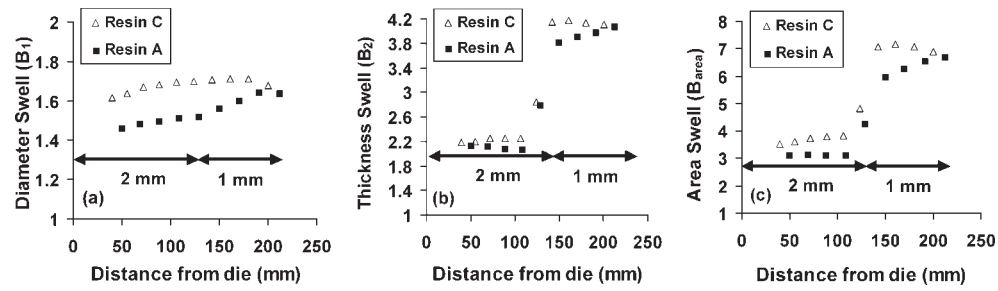


FIG. 7. Effect of parison programming on (a) diameter swell, (b) thickness swell, and (c) area swell using the die III. The arrows indicate the die gap opening for each section of the parison.

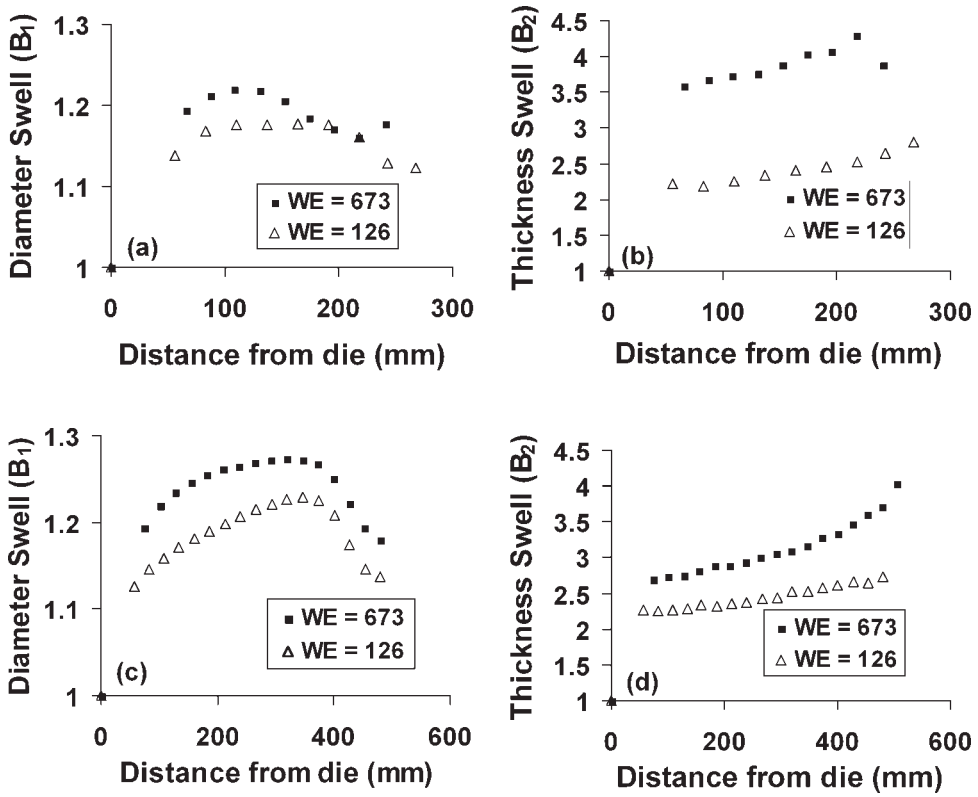


FIG. 8. Effect of WE number on (a and c) diameter swell and (b and d) thickness swell using the die VII (high shear machine). The parison length is 250 mm for (a) and (b), and 500 mm for (c) and (d).

files. These results were recorded during the extrusion of a parison using the die III, featuring a high die land contraction. The arrows indicate the die gap for each portion of the parison. It is interesting to see that the doubling of the die gap does not affect the thickness of the parison since the thickness swell is reduced by a factor of 2. This points out the need for accurate swell prediction in order to achieve a desired thickness distribution for the part through parison programming. These results also suggest that the resin C follows more rapidly the changes in the die gap because of its higher elasticity.

*High-Shear Intermittent Machine*

The diameter and the thickness swell profile for the high shear machine are shown in Figs. 8a and 8b, for a target parison length of 250 mm. As expected, the parison extruded at the WE = 673 shows higher diameter and thickness swell than the one extruded at the WE = 126. The thickness swell appears to be more sensitive to the changes in the WE number. The moderate diameter swell for the high-shear machine is related to the die angle of the bushing (see Table 3), leading to a low contraction in the die land area and as a consequence to lower elongational forces. The corresponding results for the longer parison, 500 mm, are shown in Figs. 8c and 8d. The lower thickness swell for the longer parison can be explained by the longer hang time and more pronounced sag due to gravitational loads.

*Numerical Simulations*

Fig. 9 shows the recoil factor (RF) as a function of WE number calculated by the swell model (*Eqs. 8–9*) for three different die geometries (resin A). It can be seen that the elongational forces are significantly higher for the die V, compared to the die II and VI, mainly because of the higher contraction ratio for this die in the die land area.

In Table 2, the predicted parison lengths for all the simulated cases presented in this section are compared with the corresponding experimental values. The error is

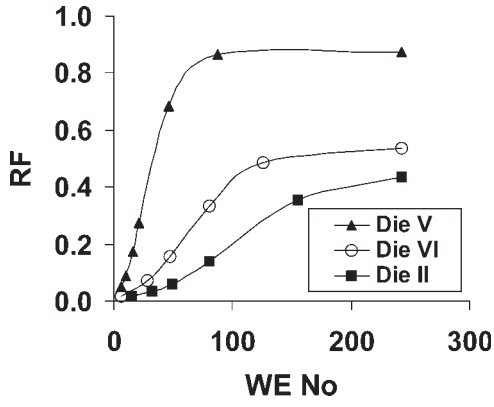


FIG. 9. Recoil factor (RF) as a function of WE number calculated by the swell model (*Eqs. 8–9*) for three different die geometries (resin A, $S_F = 0.56$, $WE_u = 304$).

 DOI 10.1002/pen

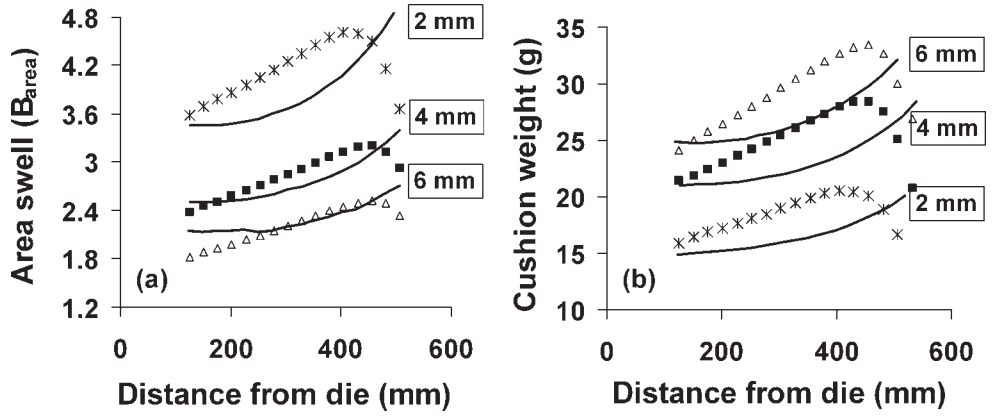


FIG. 10. Comparison of the experimental data (symbols) and the numerical predictions (lines) for the die IV at different die gap openings; (a) area swell, and (b) cushion weight profile along the parison. Numbers indicate the die gap opening.

less than 5% in most cases. The numerical prediction of the area swell for the die IV at different die gap openings is presented in Fig. 10a. These results show that the software is capable of predicting the increased area swell as the die gap decreases. However, the reduced swell at the bottom of the parison, attributed to the higher residence time in the accumulator, cannot be captured in the simulations. Therefore, the parison swell tends to increase monotonically towards the bottom as a result of the time-dependent stress relaxation. The impact of the observed discrepancy is not necessarily significant since the bottom section is usually located in the clamping zone and has a negligible effect on the final part thickness distribution. Figure 10b compares the experimental and the predicted weight profiles along the parison at different die gap openings. The sag is over-predicted to some extent in all of the cases, because of the high parison length examined in this study (550 mm). The observed discrepancies between the numerical predictions and experimental swell profiles could be reduced by extending the current swell prediction approach to a 3D finite element formulation.

The similar trends observed in Figs. 10a and 10b for the area swell and the weight profile suggest that the segment weight can be directly used to compare the parison swell/sag evolution for different die geometries or operating conditions. This makes the die design task less time consuming since either the experimental or the numerical weight profile can be used for design proposes, without the need to measure the thickness and the diameter swell using the pinch-off mold technique.

Figure 11 presents a comparison between the experimental and predicted thickness swell profiles during parison programming (see Fig. 7). These results demonstrate the potential of the software in capturing the effect of operating conditions on the parison dimensions for complex parts, mostly manufactured through parison programming. Therefore, the programming points from simulations can be readily used as a starting point for the machine profile settings, thus reducing the required time to design good parts [15].

Figure 12a shows the predicted thickness distribution for the parison formed using the die VII and for the part subsequently blow-molded (high shear machine). The corresponding experimental and predicted weight profiles for the different sections of the parison and the part, identified in Fig. 12a, are presented in Fig. 12b. It can be seen that the predicted weight distributions closely match the experimental weight profile. To validate the parison swell predictions, the experimental and the predicted thickness profiles along the part longitudinal axis are compared in Fig. 12c. The corresponding circumferential profiles for the bottom of the part are given in Fig. 12d. Once again, the predictions are in good agreement with the experimental results. In light of this, the part weight distribution can be directly used for the validation of numerical predictions where the pinch-off mold technique is not available.

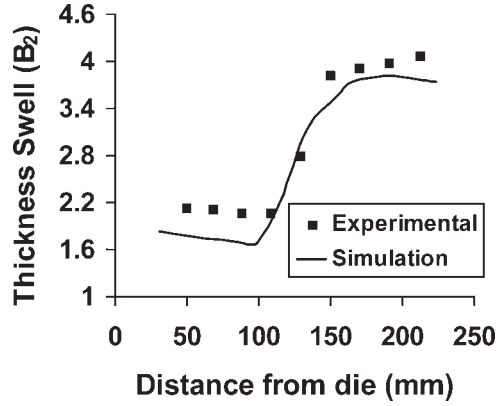


FIG. 11. Comparison of the experimental and predicted thickness swell profiles during parison programming (see Fig. 7). The arrows indicate the die gap opening for each portion of the parison.

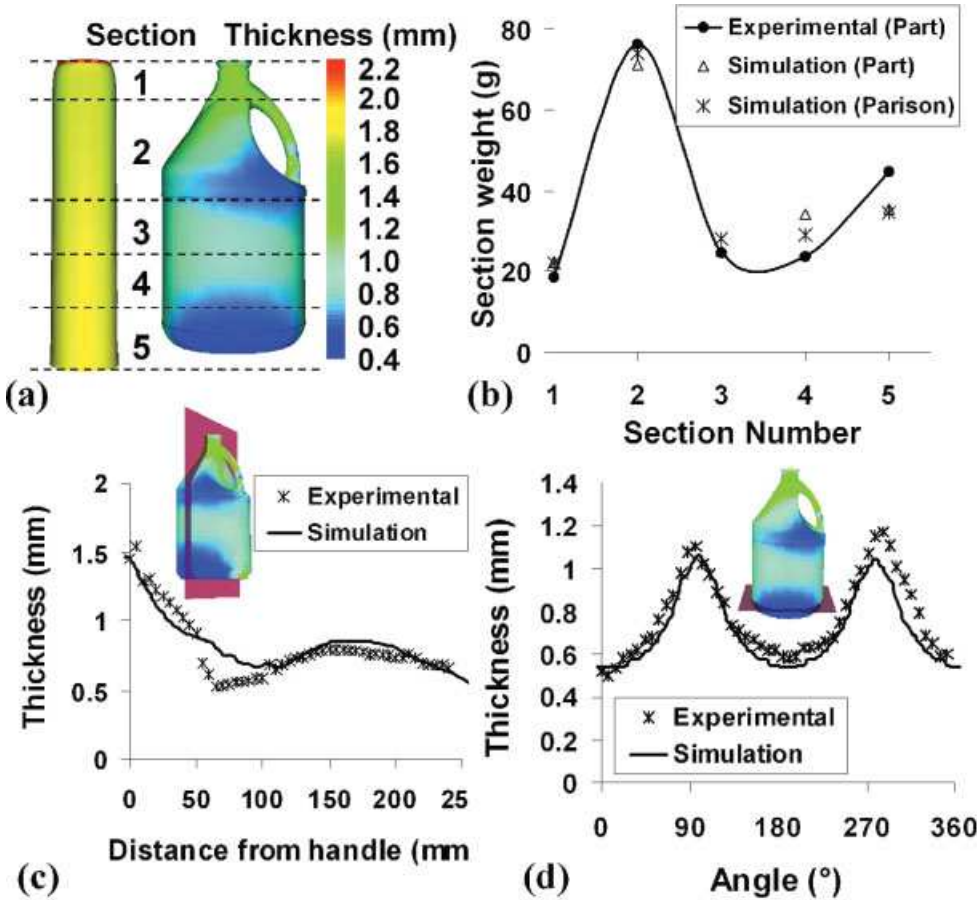


FIG. 12. Comparison of the experimental data and the numerical predictions for a parison formed using the die VII and for the blow-molded part (high shear machine: die gap = 0.8 mm); (a) thickness profile for the simulated parison and the part, (b) weight profiles for different sections of the parison and the part (c) thickness profiles along the part longitudinal axis, and (d) corresponding circumferential thickness profile at the bottom of the part. The simulated part flash is not shown. [Color figure can be viewed in the online issue, which is available at www.interscience.wiley.com.]

## CONCLUSION

This work presented the strong dependence of the parison dimensions on the material properties, the die geometry, and the operating conditions. It was shown that the resin memory and the die geometry in the die land area (contraction ratio) had the most pronounced effect on the parison swell. IMI's BlowParison software was used to predict the parison formation, taking into account the swell and sag, as well as nonisothermal effects. Parison programming with a moving mandrel and the flow rate evolution in intermittent extrusion were also considered in the numerical predictions. The part blowing and clamping for the selected case studies were performed using IMI's BlowSim software in order to validate the parison swell predictions. The comparison between the predicted parison/part dimensions and the corresponding experimental data demonstrated the efficiency of these numerical tools in predicting the final part thickness and weight distribution. The requirement for an accurate swell prediction was particularly emphasized for the parts made through parison programming. This work demonstrated that the numerical tools are the key to a better design and a better control over the thickness distribution for complex parts.

## ACKNOWLEDGMENTS

The authors thank Mario Mignacca at Petromont for his technical contribution. The technical assistance of Marc-André Rainville from IMI is also recognized.

## REFERENCES

1. N. Orbey and J.M. Dealy, *Polym. Eng. Sci.*, **24**, 511 (1984).
2. R.W. DiRaddo, A. Garcia-Rejon, L. Pecora, and D. Poirier, in SPE *ANTEC Tech. Pap.*, San Francisco, 1026 (1994).
3. N. Sheptak and C.E. Beyer, *SPE J.*, **21**, 190 (1965).
4. D. Kalyon, V. Tan, and M.R. Kamal, *Polym. Eng. Sci.*, **20**, 773 (1980).
5. R.W. DiRaddo and A. Garcia-Rejon, *Polym. Eng. Sci.*, **32**, 1401 (1992).
6. A. Garcia-Rejon and J.M. Dealy, *Polym. Eng. Sci.*, **22**, 158 (1982).

 DOI 10.1002/pen

7. D.V. Rosato and D.V. Rosato, *Blow Molding Handbook*, Hanser, New York (1989).
8. J. Vlachopoulos, *Rev. Def. Beh. Mat.*, **3**, 219 (1981).
9. M.A. Huneault, P.G. Lafleur, and P.J. Carreau, *Polym. Eng. Sci.*, **30**, 1544 (1990).
10. R.J. Koopmans, *Polym. Eng. Sci.*, **32**, 1741 (1992).
11. R.J. Koopmans, *Polym. Eng. Sci.*, **32**, 1750 (1992).
12. R.J. Koopmans, *Polym. Eng. Sci.*, **32**, 1755 (1992).
13. A.M. Yousefi, P. Collins, and R. DiRaddo, "A Comprehensive Study of Die Geometry and Operating Condition Effects on Parison Dimensions," in SPE *ANTEC Tech. Pap.*, Nashville (2003).
14. A.M. Yousefi, D. Laroche, P. Collins, and R. DiRaddo, *SPE Blow Molding Division newsletter*, Spring (2003).
15. F. Thibault, A.M. Yousefi, R.W. DiRaddo, and H. Atsbha, "Modeling of Parison Formation and Process Optimization for Blow Molded Parts," in *PPS-22 Conference*, Yamagata, Japan (2006).
16. M. Renardy, *J. Non-Newtonian Fluid Mech.*, **90**, 243 (2000).
17. M. Renardy, *Ann. Rev. Fluid Mech.*, **21**, 21 (1989).
18. R.S. Graham and T.C.B. McLeish, *J. Rheol.*, **45**, 275 (2001).
19. T.C.B. McLeish and R.G. Larson, *J. Rheol.*, **42**, 81 (1998).
20. M.J. Crochet and K. Walters, *Ann. Rev. Fluid Mech.*, **15**, 241 (1983).
21. F. Yurun and M.J. Crochet, *J. Non-Newtonian Fluid Mech.*, **57**, 283 (1995).
22. E. Brasseur, M.M. Fyrillas, G. Georgios, and M.J. Crochet, *J. Rheol.*, **42**, 549 (1998).
23. L. Douven, "Towards the Computation of Properties of Injection Moulded Products," Ph.D. thesis, Technische Universiteit Eindhoven, The Netherlands (1991).
24. F.P.T. Baaijens, *Rheol. Acta*, **30**, 284 (1991).
25. C.L. Tucker III, *Computer Modeling for Polymer Processing—Fundamentals*, Hanser, New York (1989).
26. A. Kaye, College of Aeronautics, Cransfield, Note No. 134 (1962).
27. B. Bernstein, E. Kearsley, and L.J. Zapas, *Trans. Soc. Rheol.*, **7**, 391 (1963).
28. M.L. Williams, R.F. Landel, and J.D. Ferry, *J. Am. Chem. Soc.*, **77**, 3701 (1955).
29. K.K. Kabanemi, J.F. Hetu, and A. Garcia-Rejon, *Intern. Polym. Proc.*, **12**, 182 (1997).
30. X.L. Luo and R.I. Tanner, *Int. J. Numerical Methods Eng.*, **25**, 9 (1988).
31. A.C. Papanastasiou, L.E. Scriven, and C.W. Macosko, *J. Rheol.*, **27**, 387 (1983).
32. J.M. Dealy, *Melt Rheology and its Rhole in Plastics Processing*, Van Nostrand Reinhold, New York (1990).
33. A.M. Yousefi, D. Laroche, P. Collins, and R. DiRaddo, "A Hybrid Fluid-Mechanics/Solid-Mechanics Approach for Prediction of Parison Swell in Extrusion Blow Moulding," in *6th EsaForm Conference*, Salerno, Italy (2003).
34. A.M. Yousefi, "A Combined Fluid-Mechanics and Solid-Mechanics Approach for Swell Prediction," *Technical Report* IMI-2002–93585-CNRC (2002).
35. D. Laroche, K.K. Kabanemi, L. Pecora, and R.W. DiRaddo, *Polym. Eng. Sci.*, **39**, 1223 (1999).
36. W.W. Graessley, S.D. Glasscock, and R.L. Crawley, *Trans. Soc. Rheol.*, **14**, 519 (1970).